ACS SENSORS

Article

pubs.acs.org/acssensors

Thermodynamic Charge-to-Mass Sensor for Colloids, Proteins, and Polyelectrolytes

Jos van Rijssel,[‡] Rocio Costo,[†,‡] Agienus Vrij, Albert P. Philipse,* and Ben H. Erné*

Van 't Hoff Laboratory for Physical and Colloid Chemistry, Debye Institute for Nanomaterials Science, Utrecht University, Padualaan 8, 3584 CH Utrecht, The Netherlands

ABSTRACT: A sensor is introduced that gauges the ratio of charge z to mass m of macro-ions in liquid media. The conductivity is measured in a small volume of salt solution, separated from the macro-ions by a semipermeable membrane. The mobile counterions released by the macro-ions increase the measured salt concentration, from which z/m can be calculated without any adjustable parameter. The charge sensor constitutes a noninvasive method that probes unperturbed macro-ions in a manner that is independent of (the distribution in) macro-ion size and shape. We validate the sensor's general applicability for three kinds of macro-ions, spanning 2 orders of magnitude in z/m, namely, dextran sulfate, bovine serum albumin, and colloidal silica. Measured z/m values comply for all macro-ion types with independent information on macro-ion surface charge.

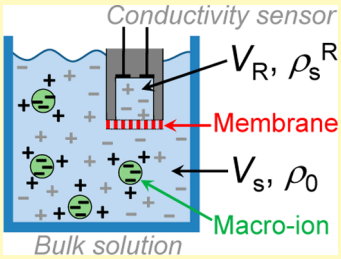

KEYWORDS: *electric charge, colloids, nanoparticles, polymers, zeta potential, conductivity, counterions, membranes*

The first determination[1,2] of the electron's charge-to-mass ratio (CMR) by Thomson in 1897, employed the classical equation of motion of electrons in vacuo with velocity v in a magnetic field B

$$dv/dt = \frac{e}{m}(v \times B) \tag{1}$$

where m is the electron mass and e is the elementary charge. After Millikan's determination[3] of e, the electron mass was obtained from the charge-to-mass ratio (CMR) in eq 1. Since Thomson's work, CMR has developed into an indispensable particle benchmark in the natural sciences, utilized in areas varying from subatomic particle detection in cloud chambers[4] to biomolecular analysis by mass spectroscopy in proteomics and biology.[5] CMR data currently also feature in studies of diverse phenomena including interstellar dust deflection by magnetic fields,[6] solid particle behavior in dusty plasmas[7] and lightning flashes caused by charged granules in wind-blown sand.[8]

In the CMR determinations referred to above, CMR is gauged via the Lorenz force on particles or (fragmented) molecules that are either in vacuo[5] or in a gas phase.[6−8] Charged macromolecules such as proteins and polyelectrolytes in solution clearly require a different CMR determination. However, a convenient, broadly employable option is still lacking, which is unfortunate since charge on colloids and polyelectrolytes (together also referred to as "macro-ions") has important consequences including the solute's colloidal stability,[9] the remarkable swelling of hydrogels[10] and the osmotic water flow in numerous physiological phenomena.[11] These consequences primarily stem from the free, mobile counterions present due to the surface charge on the macro-ions. It is these free ions that we set out to detect for determining a macro-ion's CMR, with results that are described and discussed in this paper.

Counterion counting via titration,[12] it should be noted, fails since this method determines the total number of titratable groups on polyelectrolytes rather than the fraction that actually releases a mobile counterion. Moreover, pH changes during titration may affect macro-ion conformation, whereas gauging polyelectrolytes or proteins in an unperturbed state is clearly preferable. Angle-dependent optical scattering experiments are not helpful either because (repulsions between) macro-ions dominate scattering profiles,[13] masking the weak counterion contribution. Further, the conversion of macro-ion electrophoretic mobilities from electrophoresis to a protein or polyelectrolyte valency is hardly feasible, as this conversion relies on consequential assumptions regarding the hydrodynamic size, shape, and flexibility of the polyelectrolytes and the dynamic response of their electrical double layer.[14] A more apt counterion indicator is a solution's osmotic pressure, which includes a significant ion contribution,[15] as revealed by osmotic pressure data from analytical centrifugation.[16,17] These counterion effects, however, must be disentangled from the macro-ion's partial osmotic pressure via theoretical fits.[17] Centrifugal analysis is further often hampered by sample turbidity[17,18] and macro-ion size polydispersity, complications that also affect other methods.[13,14]

Mentioned obstructions impeding counterion counting can be circumvented, at least according to recent theory,[19] via a thermodynamic approach. The proposal[19] is to gauge counterions far away from unperturbed macro-ions that, consequently, do not affect the counterion counting. The crux of the proposed method[19] is that counterion release by macro-ions to their surroundings triggers salt absorption by a sensor,

Received: August 18, 2016
Accepted: September 28, 2016
Published: September 28, 2016

DOI: 10.1021/acssensors.6b00510
ACS Sens. 2016, 1, 1344−1350

essentially a tiny solution volume connected to the macro-ion suspension via a semipermeable membrane. The increase in the sensor's salt concentration is predicted[19] to yield the macro-ion CMR without any adjustable fit parameter.

Here we report on the design and application of the first experimental prototype of the thermodynamic CMR sensor, employing impedance spectroscopy for accurate determination of the sensor's salt concentration. We validate the sensor's general applicability for three kinds of macro-ions, spanning 2 orders of magnitude in CMR, namely, dextran sulfate, bovine serum albumin, and colloidal silica. Preparation and properties of the macro-ion suspensions are described in the Materials and Methods section. Construction and performance of the sensor are presented in the Results and Discussion section, including the measurements carried out on the three model systems. First we briefly review in the next section the predicted relation[19] between sensor salt concentration and macro-ion CMR.

THEORY

The thermodynamic salt equilibrium between a macro-ion suspension and a salt solution reservoir has been analyzed[19] for arbitrary suspension and reservoir volumes. Here we will summarize the analysis for the limit of interest in this paper, namely, the sensor limit[19] in which the reservoir volume is much smaller than the suspension volume. Consider a liquid volume V_S with suspended macro-ions connected to a small salt solution volume V_R by a semipermeable membrane (Figure 1).

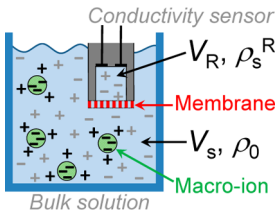

Figure 1. Schematic of the charge sensor. The salt concentration ρ_S^R in the sensor reservoir (volume V_R) is measured employing two platinum electrodes by electrical impedance spectroscopy. Neutral salt equilibrates with the sample solution (volume V_S, background salt concentration ρ_0) across a membrane that excludes macro-ions from volume V_R. According to eq 4, the ratio ρ_S^R/ρ_0 reveals the charge-to-mass ratio of the macro-ions.

Both volumes are electrically neutral phases containing homogeneously distributed, ideal ions;[15,19,20] then thermodynamic equilibrium entails[19,21] for the ionic products for salt in reservoir (index R) and suspension (index S):

$$\rho_+^R \rho_-^R = \rho_+^S \rho_-^S \tag{2}$$

where ρ_+ and ρ_- are number densities of, respectively, cations and anions. Without macro-ions, both volumes have the same initial concentration ρ_0 of salt molecules. This initial equilibrium is perturbed by adding to the suspension a weight concentration c of solutes (with mass m) that dissociate into macro-anions and z counterions (Na^+ ions in our aqueous experiments) per macro-ion. The suspension's Na^+ concentration now exceeds its equilibrium value, so sodium ions spontaneously migrate in the form of neutral salt to the salt solution to re-establish equilibrium. For large suspension volumes $V_S \gg V_R$, equilibrium ion densities in the suspension follow from their initial values ρ_0 and the number density zc/m of counterions as

$$\rho_+^S = \rho_0 + zc/m \qquad \rho_-^S = \rho_0 \qquad \text{for} \quad V_S \gg V_R \tag{3}$$

Anion densities in the large suspension volume remain constant, in contrast to the small salt solution (hereafter called a sensor) where the anion density ρ_-^S increases significantly. Because of electroneutrality, $\rho_-^R = \rho_+^R = \rho_S^R$, so the salt concentration increase in the sensor follows from eqs 2 and 3 as

$$\left(\frac{\rho_S^R}{\rho_0}\right)^2 - 1 = \left(\frac{z}{m}\right)\frac{c}{\rho_0} \qquad \text{for} \quad V_S \gg V_R \tag{4}$$

Here z/m, other than in eq 1, is the charge-number-to-mass ratio of the solutes, for brevity in what follows also denoted as CMR. The prediction from eq 4 is that the CMR of suspended macro-ions follows from the quadratic increase of the sensor's relative salt concentration against solute weight concentration c. Note that eq 1 is a kinematic expression where particle mass m enters through the particle's inertia,[22] whereas eq 4 is a purely thermodynamic one where the appearance of particle mass m has a wholly different origin: it converts the weight concentration c to the number density c/m of polyelectrolytes in solution.

Incidentally, from the analysis[19] for arbitrary solution and reservoir volumes it follows that the first-order correction term to eq 4 for a finite reservoir volume is

$$\frac{-\rho_S^R}{\rho_0} = \sqrt{1 + \left(\frac{z}{m}\right)\frac{c}{\rho_0}} + \left(\frac{V_R}{V_S}\right)\left(\frac{z}{m}\right)\frac{c}{2\rho_0} \qquad \text{for} \quad V_S \gg V_R \tag{5}$$

Note that in the sensor limit $V_R/V_S \to 0$ and eq 5 reduces to eq 4. Since $zc/(m\rho_0)$ is a number of order unity or smaller, it follows that for reservoir volumes smaller than about $V_R = 0.01V_S$ the correction term in eq 5 is wholly negligible; in our case the ratio V_R/V_S is even orders of magnitude smaller, see Results and Discussion section.

Finally we note here that, importantly, in the thermodynamic derivation of eq 4 no assumptions are made on macro-ion properties such as magnitude and polydispersity of the macro-ion mass. The small ions are assumed to behave ideally, but the same theoretical results are obtained when the assumption is made that the activity coefficient is the same for all small ions, an assumption that is generally excellent when experiments are done (as in this work) in a narrow range of ionic strength set by the background salt concentration ρ_0.

MATERIALS AND METHODS

Dextran Sulfate (DS). DS was purchased from Fluka as the sodium salt of DS with an average molecular mass of 500 kg mol^{-1} and a sulfur content of 17.8 wt %, corresponding to on average 2800 sulfate groups per DS molecule. Charge sensor measurements were performed using a Spectra/Por membrane with a MWCO of 1 kDa. Polydispersity index $p = M_w/M_n$ (M_w is the weight- and M_n the number-averaged molar mass) of dextrans is typically[23] of order $p = 2$, a value that corresponds[24] to a polydispersity in molecular mass of around 30%. Due to this substantial polydispersity a significant fraction of DS polymer segments may fall below the 1 kDa cutoff of the sensor's membrane. Therefore, DS-solution (~10 wt %) was first dialyzed for 48 h in a 12−14 kDa dialysis membrane (Spectra/Pro, Spectrum Laboratories) against a solution with an excess NaCl concentration to prevent exchange of the sodium counterions with protons. The dialyzed sample was concentrated by water evaporation and the DS weight concentration was determined employing an Anton Paar MCP 500 polarimeter at 20.00 °C. Calibration samples for DS-to-

DOI: 10.1021/acssensors.6b00510
ACS Sens. 2016, 1, 1344−1350

water mass fraction of 0.6×10^{-4} to 5.2×10^{-4} indicated the following specific rotations of DS: 279.5°/dm at 365 nm, 186.3°/dm at 436 nm, 114.0°/dm at 546 nm, and 96.2°/dm at 589 nm. In all sensor experiments on DS the polymer was dissolved in aqueous solutions at pH = 6.9 with an initial salt concentration of 1.00 mM NaCl.

Titrations. Conductivity and pH of DS solutions were measured with a calibrated Mettler Toledo pH meter. A solution of 1.00 μM dialyzed dextran sulfate in 1.00 mM NaOH was titrated at 22.5 °C with 1.00, 0.010, and 0.001 M HCl solutions depending on the pH range. The amount of H^+ required to change the pH was compared for 1.00 mM NaOH with and without 1 μM of DS (see Figure 2a). The difference is small, especially at low pH (see Figure 2b). A plateau is found at pH 3 to 2, indicating a charge of $z = 1200 \pm 160$. By starting at high pH, we ensure that all chargeable groups were dissociated and could be neutralized with H^+; in our other experiments, the counterions are Na^+ and DS is at neutral pH, where most groups that can dissociate are indeed dissociated. The difficulty of determining the charge by titration is clear from the fact that most of the added H^+ is already necessary without added DS, so that the error in the additional amount of H^+ required due to 1 μM DS is high. Moreover, the method relies on the validity of the measured pH, which is uncertain. Adsorption of DS to the outer porous glass bulb of a pH electrode may affect the electrical potential drop at the porous glass/solution interface.[25]

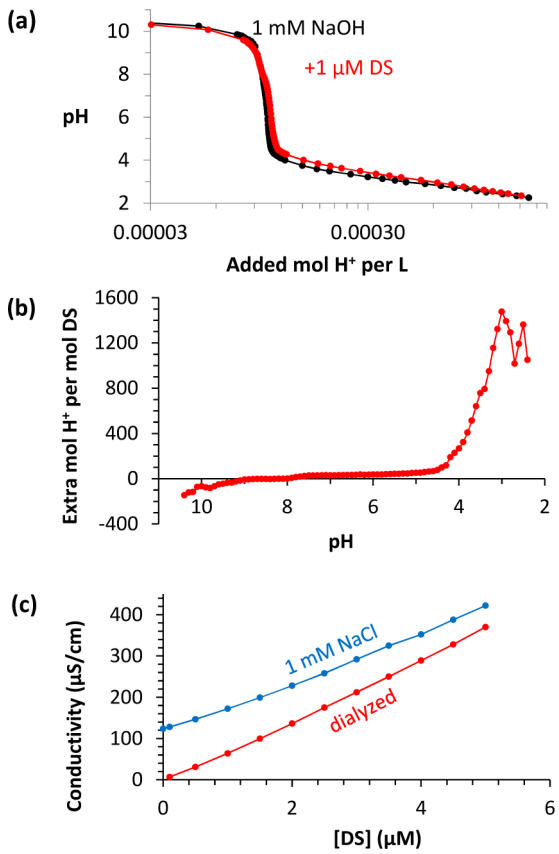

Figure 2. (a) Moles of HCl required to decrease the pH of 1 mM NaOH solutions without and with 1 μM of dextran sulfate (DS). The curves were shifted along the x-axis to coincide with each other at pH 8 to 9, where we assume DS to be uncharged. (b) Extra amount of HCl required to change the pH, per mol of added DS, obtained by interpolation of the data in (a). (c) Electrical conductivity as a function of DS concentration after dialysis and after addition of 1 mM NaCl.

Conductivity. In view of the difficult interpretation of titration results, we also studied DS by the electrical conductivity of a DS bulk solution (see Figure 2c). Without DS, 1.00 mM NaCl—corresponding to 2000 μM of ions—has a conductivity of 124 μS/cm, and to reach the same conductivity with DS in pure water, the required polymer concentration is 1.75 μM. This can be interpreted as due to 2000/1.75 = 1142 charges with a mobility on the same order as that of Na^+ and Cl^-. On the assumption that the polyelectrolyte backbone has a negligible contribution to the conductivity, 1142 is the number of counterions of sulfate groups per polyelectrolyte chain, similar to the charge found from titration. When the DS concentration increases from 0 to 5 μM, the effect of adding 1 mM NaCl decreases by a factor of 2, in line with the occurrence of ion condensation.

Bovine Serum Albumin (BSA). BSA "fraction V" was used as received from Roche Diagnostics. A stock solution of 200 g/L was prepared by mixing 2 g of BSA crystals with 10 mL of background salt solution, placing the sealed vial on a rotating stage until BSA is dissolved. The aqueous stock solution of BSA at pH = 6.9 in 0.5 mM NaCl was filtered using a 200 nm Millipore filter to remove any aggregates and the final concentration was measured using a PerkinElmer Lambda 35 UV−vis spectrophotometer from the absorbance at 280 nm. In all sensor experiments on BSA the protein was dissolved in aqueous solutions at pH = 6.9 with an initial salt concentration of 1.00 mM NaCl.

Colloidal Silica (CS). CS particles with an average diameter of 10.9 nm (see Figure 3) were delivered in an aqueous dispersion (trade name Bindzil, from Akzo Nobel, Sweden). Silica nanoparticles significantly dissolve in water[24] making the ionic strength ill-defined; aqueous dispersions usually also turn into a gel in the course of time. Therefore, the CS-particles were coated with 3-methacryloxypropyltrimethoxysilane (TPM) and transferred to analytical grade ethanol.[13,24] Negatively charged TPM-coated silica particles have an almost unlimited colloidal stability in ethanol;[13,16] ionic strength can be tuned by addition of (fully dissociating[13,16]) $LiNO_3$. A stock dispersion of TPM-coated CS-particles in ethanol was centrifuged twice for 16 h at 3800g followed by redispersal of the silica sediment in ethanol. Finally, the CS-particles were stored in absolute ethanol containing 0.25 mM $LiNO_3$. The solid content of 4.58 wt % of the dispersion was determined by drying weighed dispersion samples to constant weight.

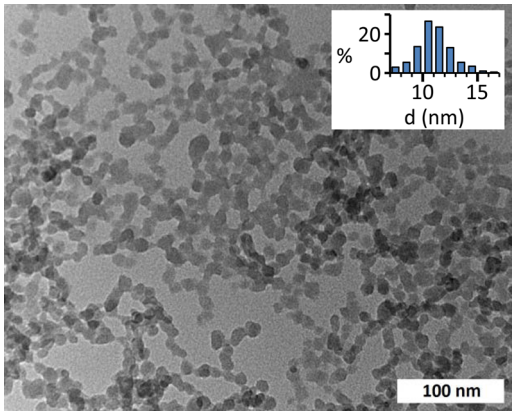

Figure 3. Electron micrograph of the colloidal silica particles, sintered together in the electron microscope. The particles have an average diameter of 10.9 nm as determined from the size distribution in the inset.

For charge sensor measurements on CS the sensor was sealed with a 1 kDa membrane suitable for use in ethanol (Spectra/Por 6) and equilibrated in the 0.25 mM $LiNO_3$ background ethanol solution until the resistance in the sensor volume was constant. The sensor was transferred to the stock CS-dispersion, and to vary the silica concentration once equilibrium was attained, different amounts of CS-suspension were removed and replaced with 0.25 mM $LiNO_3$ solution.

Impedance Spectroscopy. To quantify salt concentrations in a sensor compartment (Figure 4) spectra of the electrical impedance spectra between two platinum electrodes were measured in the

DOI: 10.1021/acssensors.6b00510
ACS Sens. 2016, 1, 1344−1350

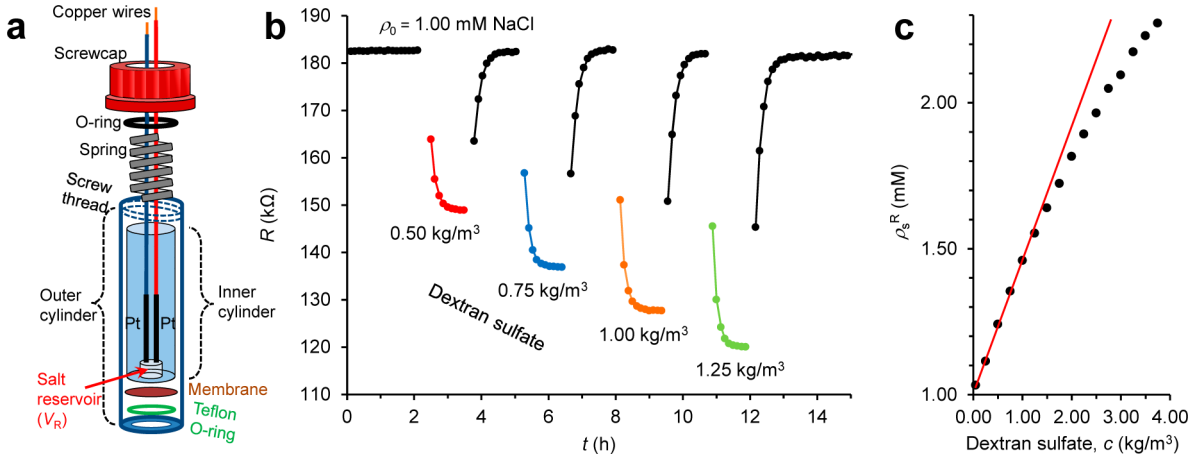

Figure 4. (a) Design of the home-built charge-to-mass sensor. Two copper wires connected to the impedance analyzer are soldered to two platinum wires (Pt) ending in a space (drilled into a glass inner cylinder) containing the small salt solution volume V_R, appearing in the derivation of eq 4. An outer cylinder, a screwcap, and a metal spring fix the membrane and a flat Teflon O-ring into place. (b) Typical sensor resistance R versus time plots, here for dextran sulfate (DS) with weight concentrations as indicated. Upon DS addition to the suspension, R decreases until thermodynamic equilibrium is reached, after which R returns to its initial value for the background 1 mM NaCl solution, with no signs of hysteresis. Note that R descent toward equilibrium becomes more pronounced at higher SD concentrations, as predicted by eq 4. (c) Typical nonlinear increase of the sensor salt concentration as a function of dextran sulfate concentration.

frequency range of 1 Hz to 100 kHz with 10 frequencies per decade, using an 8-channel PMC 1000 potentiostat from PAR. The root-mean-square amplitude of the applied potential was merely 20 mV, to avoid electrochemical change. The solutions were maintained at 20.0 °C in thermostated jacketed beakers connected to a cryostat (F25-ME refrigerated/heating circulator from Julabo). Samples were continuously stirred at 700 min^{-1} with a magnetic stirrer. Impedance spectra were fitted following ref 30 in terms of a constant-phase element in series with a resistor of magnitude R that is in parallel with a capacitor of magnitude C

$$Z(\omega) = \frac{R - i\omega RC}{1 + \omega^2(RC)^2} + \frac{1}{q_0\omega^n}\exp\left[-i\frac{\pi}{2}n\right] \tag{6}$$

where Z is the electrical impedance, ω is the radial frequency, q_0 gives the impedance of the constant-phase element at $\omega = 1/\mathrm{s}$ and n is a parameter that describes the mixture of resistive and capacitive behavior of the electrical double layer near the electrodes.

RESULTS AND DISCUSSION

In this section, first the design and operation of the sensor are discussed, including geometry, dimensions, effects of membrane and diffusion on the equilibration time, and calibration. Finally, the sensor is tested on three model systems with charged macro-ions.

Sensor Geometry. Our experimental sensor (Figure 4a) comprises a salt solution volume $V_R = 5\ \mu$L, containing two Pt electrodes to determine the salt concentration via electrical impedance spectroscopy (see previous section). The macro-ion solution volume is $V_S = 20$ mL, such that the required inequality $V_S \gg V_R$ in eq 4 clearly holds.

The sensor's geometry and design require careful optimization in view of, among other things, shortening salt equilibration times (Figure 4b) and ensuring that electric field lines remain confined to the sensor's interelectrode space. Compared to our geometry with two coplanar electrodes, two parallel electrodes facing each other might theoretically be better, because they would result in straighter field lines from one electrode to the other, avoiding electrokinetic effects at the walls of the compartment. However, we were able to implement our geometry without using any glue, rendering the probe much more robust chemically than our earlier attempts with a theoretically better geometry but with glue. To evaluate the effect of overshoot of the electrical field lines beyond the measurement compartment, we performed experimental tests and theoretical calculations.

Compartment Depth. Experimentally, compartments of different depths d were realized, and the resistance of a salt solution was measured, first with the compartment sealed hermetically using a glass cover, and second with the probe immersed without membrane in bulk salt solution. The ratio of the thus measured two resistances is unity when the field lines are confined to the compartment. Figure 5b demonstrates that the depth should not be less than 1 mm, preferably $d = 2$ mm, for the sensor to measure almost exclusively on the solution inside the measurement compartment.

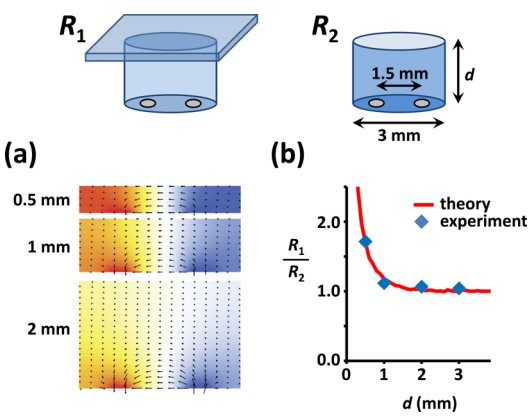

Figure 5. Effect of the depth d of the measurement compartment on the resistance measured between the two electrodes. R_1 is measured with the compartment sealed by a glass plate and R_2 with the compartment open to bulk solution. (a) Electrical potential distribution in the vertical midplane of the sensor volume for three different depths d in a sealed compartment. (b) Ratio of R_1 to R_2 from theory and experiment as a function of d. A ratio of 1 indicates that the electric field lines are confined to the measurement compartment.

DOI: 10.1021/acssensors.6b00510
ACS Sens. 2016, 1, 1344−1350

Electric Field Calculations. The overshoot effect is accounted for quantitatively by a two-dimensional model of the measurement compartment, describing the spatial distribution of the electrical potential in the vertical plane that connects the electrodes (Figure 5a). The Poisson equation was solved for finite volume elements using Mathematica 10: $-\varepsilon\nabla^2\phi = 0$ (zero free charge density, as the measurement compartment contains only neutral salt solution, with equal concentrations of free positive and negative ions), where ε is the dielectric constant of the medium, ∇^2 is the Laplacian operator and ϕ is the electric potential. The gradient of ϕ is the field E. The walls of the probe are made of nonconductive glass, and therefore E is zero perpendicular to the glass boundaries. Together with the known potentials at the electrodes, these boundary conditions give a unique solution of the electric potential in each volume element. Given the conductivity σ of an electrolyte solution, the resistance by the sensor follows from the applied voltage and from the total current between the electrodes, calculated by integrating local currents $J = \sigma E$ over the finite volume elements contacting either electrode. The main additional insights provided by theory is that the extent to which the field lines are confined to the measurement compartment is independent of ionic strength and that, to avoid the overshoot effect in our current geometry, the compartment depth should be at least on the order of the distance between the electrodes.

Diffusion Times. The depth of the measurement compartment also strongly affect equilibration times. When the probe is inserted into a suspension, the solution inside the measurement compartment must adapt its salt concentration by ion transfer across the membrane and diffusive ion transport inside the compartment. From a compartment depth of 2 mm and typical diffusion coefficients of $D \sim 1.5 \times 10^{-9}$ m^2 s^{-1} for aqueous ions at room temperature, the characteristic time of diffusion-limited equilibration is expected to be 45 min. In practice equilibration times, as illustrated by Figure 4b, can be much longer because of slow ionic transfer across the, presumably charged, membranes.

Membrane. To prepare our home-built sensor for measurements, first it was held upside down and the measurement compartment (volume V_R in Figure 4a) was filled with the background salt solution, allowing any air bubbles to escape. Second, the membrane—previously equilibrated with the same background salt solution—was placed on top of the measurement compartment. Finally, the O-ring was placed on top of the membrane and the probe was closed by screwing it onto the second glass cylinder. The membrane was a disk cut from dialysis tubing. Although membranes with a molecular weight cut off (MWCO) on the order of 100 Da might seem appropriate, given the sizes of small ions like Na^+ and Cl^-, ion transport through the narrow pores of 100 Da membranes may slow down considerably due to electrostatic effects. For cellulose membranes it was shown[26] that diffusive transport of aqueous NaCl can be retarded by orders of magnitude in small pores (2 kDa) at low ionic strengths (<10 mM). Therefore, the MWCO here was chosen just sufficiently low to prevent permeation of macrosolutes.

Sensor Calibration. Before individual sensors could be used to determine salt concentration ρ_S^R in the sensor volume, they were each calibrated at 20.0 °C. Temperature control is important owing to the significant temperature dependence of ionic mobilities,[27] changing by about 5% per °C in water. In the impedance spectra, electrode polarization dominated at low frequencies, capacitive behavior dominated at the highest frequencies (for low-conductivity samples), and impedance was mainly resistive in an intermediate frequency range. As expected from literature data for the concentration dependence of ionic conductivities,[27] the measured resistance R was almost but not precisely inversely proportional to salt concentration ρ_S, an effect that we also found with commercial conductivity probes. Our calibration data for different individual sensors in salt solutions could be fitted excellently according to

$$\log_{10}(R/\mathrm{k\Omega}) = A \log_{10}(\rho_S/\mathrm{mM}) + B \tag{7}$$

with values of fit parameters A and B given in the legend of Figure 6.

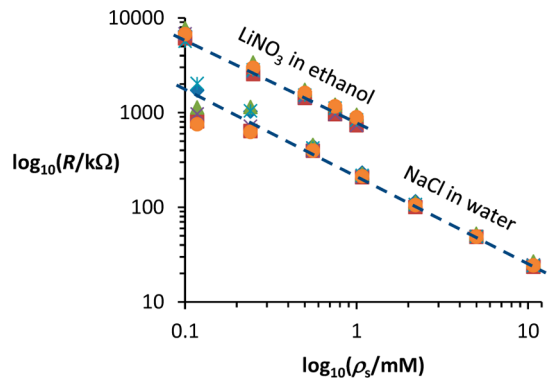

Figure 6. Calibrations of the sensor in water and ethanol. Resistance R versus salt concentration ρ_S measured for 6 different sensor probes and fitted to eq 7 for solutions of $LiNO_3$ in ethanol ($A = -0.91 \pm 0.05$, $R = 824 \pm 75$ kΩ at 1 mM) and aqueous NaCl solutions ($A = -0.956 \pm 0.015$, $R = 234 \pm 11$ kΩ at 1 mM). The data scatter for aqueous solutions with less than 0.4 mM of added salt stems from additional ions due to dissolution of atmospheric CO_2.

Sensor Measurements on Macro-Ion Systems. Figure 4b shows typical sensor data, sensor resistance R against time t, here for various dextran sulfate (DS) concentrations in water with an initial salt concentration of $\rho_0 = 1.00$ mM NaCl. Figure 4b clearly illustrates the reversibility of the sensor: upon each DS addition the sensor's resistance R decays to a new equilibrium value and upon replacement of the suspension by pure salt solution, R reverts to its initial level just above $R = 180$ kΩ. When a new DS-dose is added, the cycle repeats itself, with the resistivity descending to lower equilibrium values at higher DS-concentrations. The cycling in Figure 4b and absence of any hysteresis unambiguously demonstrate thermodynamic salt equilibrium between suspension and sensor, and its adaption to counterion release by DS.

Figure 4c shows the typical sensor's salt concentration increase, obtained from resistivity data versus DS weight concentration. Striking is the significant sensor response to DS concentrations as low as $c \approx 0.25$ kg/m^3. Further, the response in Figure 4c clearly becomes nonlinear at concentrations above $c \approx 1.5$ kg/m^3. This is the nonlinearity predicted by eq 4, as demonstrated by Figure 7, revealing that sensor readings for dextran sulfate, BSA, and colloidal silica all obey the quadratic dependence from eq 4. According to eq 4, the slope in Figure 7 equals the CMR so Figure 7 directly shows that the CMR of colloidal silica is about 2 orders of magnitude below that of dextran sulfate, with an intermediate CMR for BSA proteins.

The relatively high CMR of dextran sulfate follows quite accurately from the linear fit in Figure 7 with an uncertainty of only a few percent (Table 1). The colloidal silica data in Figure

DOI: 10.1021/acssensors.6b00510
ACS Sens. 2016, 1, 1344−1350

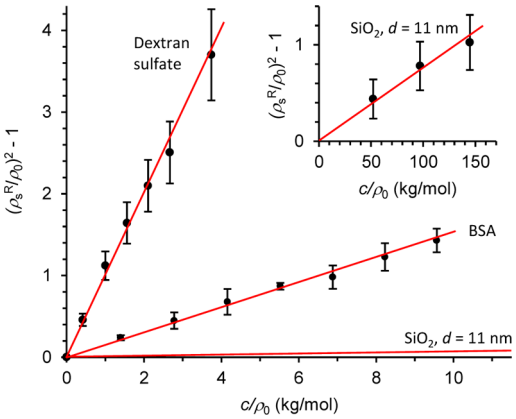

Figure 7. Results for the relative salt concentration ρ_S^R/ρ_0 as a function of the macro-ion weight concentration c in suspension, plotted according to eq 4. In the figure's horizontal axis, ρ_0 is a molar salt concentration such that slopes are equal to a charge number to mass ratio (CMR) in the form z/M, where M is the macro-ion molar mass. The slopes indicate that for colloidal silica (CS) the CMR is 2 orders of magnitude below that of dextran sulfate (DS), with an intermediate CMR for bovine serum albumin (BSA) (see also Table 1). Error bars for DS and BSA stem from triplicate series of experiments, for CS (see inset) mainly from the uncertainty in the background concentration of $LiNO_3$ in the volatile ethanol.

7 are noisy due to the very low CMR of colloidal silica (Table 1). In addition, equilibration times were much longer than in water due to the slower diffusion of small ions in ethanol and probably also due to slower ion exchange across the membrane. Moreover, evaporation of ethanol could not be prevented completely during prolonged measurements, leading to an uncertainty of 5% in the background salt concentration, reflected by the size of the error bars in Figure 7.

Just as for the kinetic CMR determination via eq 1, to unlock the CMR, separate information is needed, in our case the mass of a colloid or polyelectrolyte rather than its charge. In our analyses here, we will assume that z is independent of macro-ion concentration. Finding the charge number z per molecule is straightforward for the well-defined mass of the monodisperse BSA (Table 1). The outcome for the BSA charge number from the sensor data is $z = 10.4 \pm 0.4$ at pH = 6.9, which is only slightly below the value $z \approx 11$ from BSA titrations at pH = 7.3.[28] This $z \approx 11$, incidentally, also accounts for the magnitude of electroviscous effects in BSA solutions.[28] Our result $z = 10.4 \pm 0.4$ at pH = 6.9 is also quite close to the BSA net charge number $z = 8.4 \pm 0.3$ at pH= 6.8 that has been derived from dynamic NMR data.[29]

For the polydisperse DS we employ its number-averaged molar mass (Table 1) to obtain $z = 494 \pm 15$, a value significantly below the total number of about 1200 titratable sulfate groups reported in section 3. This implies that only about 41% of sulfate groups releases a mobile Na^+ ion, with other counterions "condensed" on, or remaining in the vicinity of, a DS molecule.

For the colloidal silica in ethanol we find that CS-particles on average release a mere $z = 3.7 \pm 1.5$ mobile counterions. An estimate for the charge number on the CS-particles based on electrophoresis is as follows. Electrophoretic mobility measurements on CS-particles by laser-Doppler electrophoresis (Malvern Zetasizer Nano) yields a zeta-potential of $\zeta = -45 \pm 25$ mV. Equating the electrical force on a silica particle to the hydrodynamic drag force yields

$$z = \frac{6\pi\varepsilon_0\varepsilon_r\zeta}{e} \tag{8}$$

where r is the hydrodynamic radius, ε_0 is the permittivity of free space, ε_r is the dielectric constant of ethanol, and e is the positive elementary charge. The outcome $z = 6 \pm 4$ complies with the value 3.7 ± 1.5 (Table 1) from the sensor experiments.

CONCLUSION

In conclusion, we have demonstrated that the absolute charge-to-mass ratio (CMR) of dissolved macro-ions can be determined quite accurately with our first, home-built prototype of a thermodynamic sensor. The charge sensor constitutes a noninvasive method that probes unperturbed macro-ions in a manner that is independent of (the distribution in) macro-ion size and shape. The dependence in eq 4 of the sensor's salt increase on macro-ion concentration applies quantitatively to the investigated colloids, proteins, and polyelectrolytes. Measured CMR values comply for all macro-ion types with independent information on macro-ion surface charge. Future applications of the CMR sensor include ion condensation on charged biopolymers and other polyelectrolytes and colloids, monitored by sensor salt concentration decrease. Moreover, sensors could be developed not based on conductivity measurements but with ion-specific electrodes to examine more complex gels or tissues that harbor electrolyte mixtures.

AUTHOR INFORMATION

Corresponding Authors

*E-mail: b.h.erne@uu.nl.

*E-mail: a.p.philipse@uu.nl.

Present Address

†Instituto de Ciencia de Materiales de Madrid (CSIC), Sor Juana Inés de la Cruz 3, 28049 Madrid, Spain

Author Contributions

‡These authors contributed equally.

Notes

The authors declare no competing financial interest.

Table 1. Macro-Ion Charge-to-Mass Ratios and Particle Charge Numbers

	z/M[a] mol kg^{-1}	M kg mol^{-1}	z[b] (sensor)	z
Dextran sulfate (DS)	$99(\pm3) \times 10^{-2}$	500 ± 150[c]	494 ± 15	1200[d]
Bovine serum albumin (BSA)	$156(\pm6) \times 10^{-3}$	68[e]	10.4 ± 0.4[f]	11[g] 8.4 ± 0.3[h]
Colloidal silica (CS)	$59(\pm12) \times 10^{-4}$	630 ± 252[i]	3.7 ± 1.5	6 ± 4[j]

[a]From the slopes of the thermodynamic sensor data in Figure 7; M is the macro-ion molar mass. [b]Charge number per molecule or silica particle from the charge sensor. [c]Polydispersity estimated from typical dextran polydispersity indices.[23] [d]Total number of titratable groups. [e]Supplier's information. [f]At pH = 6.9. [g]Titration at pH = 7.3.[28] [h]From dynamic NMR data at pH = 6.8.[29] [i]From average CS particle radius 10.9 (±1.6) nm, see Figure 3, and mass density $\delta = 1.6$ (±0.1) g cm^{-3} of TPM-coated silica.[13] [j]Charge number estimated from silica surface potential.[13]

DOI: 10.1021/acssensors.6b00510
ACS Sens. 2016, 1, 1344−1350

ACKNOWLEDGMENTS

Henkjan Siekman and Stephan Zevenhuizen are thanked for their help in realizing the charge sensor and Joeri Opdam for the sensor measurements on colloidal silica. Per Linse is acknowledged for discussions on the thermodynamics underlying the charge sensor. This work is supported financially by the Dutch Technology Foundation STW (project 11020-2) which is part of The Netherlands Organization for Scientific Research (NWO), via the STW/Hyflux Partnership Program.

REFERENCES

(1) Thomson, J. J. Cathode Rays. *Philos. Mag.* **1897**, *44*, 293−316.
(2) Thomson, J. J. *Rays of Positive Electricity and their Application to Chemical Analysis*; Longmans: London, 1913.
(3) Millikan, R. A. *The Electron: Its Isolation and Measurements and the Determination of Some of its Properties*; The University of Chicago Press: Chicago, 1917.
(4) Braibant, S.; Giacomelli, G.; Spurio, M. *Particles and Fundamental Interactions: An Introduction to Particle Physics*; Springer: Heidelberg, 2009.
(5) Aebersold, R.; Mann, M. Mass Spectrometry-Based Proteomics. *Nature* **2003**, *422*, 198−207.
(6) Ma, Q.; Matthews, L.; Land, V.; Hyde, T. Charging of Interstellar Dust Grains Near the Heliopause; DOI: arxiv.org/pdf/1107.0283; 2011.
(7) Ganguli, G.; Merlino, R.; Sen, A. *29. Oscillations in a Dusty Plasma Medium. Review of Radio Science 1999−2002*; Stone, R. W., Ed; Institute of Electrical and Electronic Engineers, 2002; pp 683−719.
(8) Bo, T. L.; Zhang, H.; Zheng, X. Charge-to-Mass Ratio of Saltating Particles in Wind-Blown Sand. *Sci. Rep.* **2014**, *4*, 5590 DOI: 10.1038/srep05590.
(9) Evans, D. F.; Wennerström, H. *The Colloidal Domain: Where Physics, Chemistry, Biology and Technology Meet*; Wiley-VCH, 1998.
(10) Edgecombe, S.; Schneider, S.; Linse, P. Monte Carlo Simulations of Defect-Free Cross-Linked Gels in the Presence of Salt. *Macromolecules* **2004**, *37*, 10089−10100.
(11) Rose, B. D.; Post, T. W. *Clinical Physiology of Acid-Base and Electrolyte Disorders*; McGraw-Hill: New York, 2001.
(12) Jones, I.; Atkins, P. *Chemistry; Molecules, Matter, and Change*; W. H. Freeman and Company: New York, 2000.
(13) Philipse, A. P.; Vrij, A. Determination of Static and Dynamic Interactions between Monodisperse, Charged Silica Spheres in an Optical Matching Organic Solvent. *J. Chem. Phys.* **1988**, *88*, 6459−6470.
(14) Delgado, A. V.; Gonzalez-Caballero, F.; Hunter, R. J.; Koopal, L.; Lyklema, J. Measurement and Interpretation of Electrokinetic Phenomena. *J. Colloid Interface Sci.* **2007**, *309*, 194−224.
(15) Philipse, A. P.; Vrij, A. The Donnan equilibrium I. On the Thermodynamic Foundation of the Donnan Equation of State. *J. Phys.: Condens. Matter* **2011**, *23*, 194106−194117.
(16) Rasa, M.; Philipse, A. P. Evidence for a Macroscopic Electric Field in the Sedimentation Profiles of Charged Macromolecules. *Nature* **2004**, *429*, 857−860.
(17) Rasa, M.; Erné, B.; Zoetekouw, B.; van Roij, R.; Philipse, A. P. Macroscopic Electric Field and Osmotic Pressure in Ultracentrifugal Sedimentation-Diffusion Equilibria of Charged Colloids. *J. Phys.: Condens. Matter* **2005**, *17*, 2293−2314.
(18) Luigjes, B.; Thies-Weesie, D. M. W.; Philipse, A. P.; Erné, B. Sedimentation Equilibria of Ferrofluids. I. Analytical Centrifugation in Ultrathin Glass Capillaries. *J. Phys.: Condens. Matter* **2012**, *24*, 245103−245111.
(19) Philipse, A. P.; Kuipers, B. M. W.; Vrij, A. A Thermodynamic Gauge for Mobile Counter-Ions from Colloids and Nanoparticles. *Faraday Discuss.* **2015**, *181*, 103−121.
(20) Philipse, A. P.; Kuipers, B. M. W.; Vrij, A. Algebraic Repulsions between Charged Planes with Strongly Overlapping Electrical Double Layers. *Langmuir* **2013**, *29*, 2859−2870.
(21) Denbigh, K. *The Principles of Chemical Thermodynamics*; Cambridge UP: Cambridge, 1959.
(22) Jackson, J. D. *Classical Electrodynamics*; John Wiley & Sons: New York, 1975.
(23) Granath, K. A. Solution Properties of Branched Dextran. *J. Colloid Sci.* **1958**, *13*, 308−328.
(24) Philipse, A. P. Particulate Colloids; Aspects of Preparation and Characterization, In *Fundamentals of Colloids and Interface Science*, Lyklema, J.Ed.; Elsevier: Amsterdam, 2005; Vol. *IV*.
(25) Harris, D. C. *Quantitative Chemical Analysis*; W. H. Freeman & Co: New York, 2010.
(26) Romero, V.; Vazquez, M. I.; Benavente, J. Study of Ionic and Diffusive Transport through a Regenerated Cellulose Nanoporous Membrane. *J. Membr. Sci.* **2013**, *433*, 152−159.
(27) Gunning, H. E.; Gordon, A. R. The Conductance and Ionic Mobilities for Aqueous Solutions of Potassium and Sodium Chloride at Temperatures from 15° to 45°C. *J. Chem. Phys.* **1942**, *10*, 126−131.
(28) Tanford, C.; Buzzell, J. G. The Viscosity of Aqueous Solutions of Bovine Serum Albumin between pH 4.3 and 10.5. *J. Phys. Chem.* **1956**, *60*, 225−231.
(29) Böhme, U.; Scheler, U. Effective Charge of Bovine Serum Albumin Determined by Electrophoresis NMR. *Chem. Phys. Lett.* **2007**, *435*, 342−345.
(30) Kortschot, R. J.; Philipse, A. P.; Erné, B. H. Debye Length Dependence of the Anomalous Dynamics of Ionic Double Layers in a Parallel Plate Capacitor. *J. Phys. Chem. C* **2014**, *118*, 11584−11592.

DOI: 10.1021/acssensors.6b00510
ACS Sens. 2016, 1, 1344−1350